frontiers in Earth Science

ORIGINAL RESEARCH
published: 16 April 2021
doi: 10.3389/feart.2021.650014

Compositional Variation of Amphiboles During Magma Mixing: A Case Study of Huangyangshan A-Type Granite in Kalamaili Metallogenic Belt, East Junggar, China

Chenyang Ye[1,2,3,4,5], Yonggang Feng[1,2], Ruxiong Lei[1,2] and Gaoxue Yang[1,2]*

[1] School of Earth Science and Resources, Chang'an University, Xi'an, China, [2] Laboratory of Mineralization and Dynamics, Chang'an University, Xi'an, China, [3] State Key Laboratory of Lithospheric Evolution, Institute of Geology and Geophysics, Chinese Academy of Sciences, Beijing, China, [4] College of Earth and Planetary Sciences, University of Chinese Academy of Sciences, Beijing, China, [5] Innovation Academy for Earth Science, Chinese Academy of Sciences, Beijing, China

OPEN ACCESS

Edited by:
Xiaohua Deng, Beijing Institute of Geology for Mineral Resources, China

Reviewed by:
Huan Li, Central South University, China
Fuquan Yang, Chinese Academy of Geological Sciences (CAGS), China
Ewa Słaby, Institute of Geological Sciences, Polish Academy of Sciences, Poland

***Correspondence:**
Yonggang Feng
ygfeng@chd.edu.cn

Specialty section:
This article was submitted to Economic Geology, a section of the journal Frontiers in Earth Science

Received: *06 January 2021*
Accepted: *29 March 2021*
Published: *16 April 2021*

Citation:
Ye C, Feng Y, Lei R and Yang G (2021) Compositional Variation of Amphiboles During Magma Mixing: A Case Study of Huangyangshan A-Type Granite in Kalamaili Metallogenic Belt, East Junggar, China. Front. Earth Sci. 9:650014. doi: 10.3389/feart.2021.650014

The Huangyangshan A-type granitic pluton, distributed along the thrust fault in the Kalamaili region of East Junggar, Xinjiang, China, consists of alkaline granite containing abundant dioritic enclaves that formed via magma mixing. Both the host granite and the enclaves contain sodic amphiboles. The textural evidence indicates that amphiboles crystallized as a magmatic phase in both units. We determined major and trace element contents of amphiboles from both units to investigate the compositional variation of the amphiboles during the magma mixing process. The results show that cations of W- and C-site are influenced by chemical compositions of the magma whereas cations of A-, B- and T-site and Al^{3+} are controlled by crystal structure. Therefore, the variations of W- and C-site cations can reflect magma evolution. The core and rim of the amphiboles show similar trace element patterns, which also suggests that the amphiboles are late-stage phases. Furthermore, the amphibole-only thermometers yield reasonable estimates that are consistent with petrographic evidence. However, thermometers based on partition coefficients and all the currently available amphibole-based barometers that rely on Al contents or D_{Al} cannot be applied to Fe-rich and Al-poor amphiboles.

Keywords: amphibole, A-type granite, dioritic enclave, magma mixing, Sn mineralization, Huangyangshan

INTRODUCTION

Magma mixing is a common magmatic process during formation of granitoids (Kumar et al., 2004; Liu et al., 2013; Xiong et al., 2020). Previous studies suggest that magma mixing can be important for formation of critical metal deposits (e.g., Ma et al., 2013). If mafic magma injects into felsic magma during magma mixing, microgranular mafic enclaves (MMEs) would likely form. During this process, amphiboles are usually the major rock-forming minerals.

The amphibole-group are complex in chemical composition but share a general chemical formula expressed as $AB_2C_5T_8O_{22}W_2$, where A, B, C, and T represent different crystal cites (Leake et al., 1997). The T site is commonly occupied by Si^{4+}, Al^{3+}, Ti^{4+}, and the like and is tetrahedrally coordinated, forming a double chain of tetrahedra. The A site occurs in the center of space between the double-chains of the structure. The C site is octahedrally coordinated and occupied by cations including Mg^{2+}, Fe^{2+}, Mn^{2+}, Al^{3+}, Fe^{3+}, Mn^{3+}, Ti^{4+}, etc. Cations on the B-site situate at the periphery of the strip of the octahedra C-cations occupy. Anions including OH^-, F^-, Cl^-, and O^{2-} dominate the W-site. This complexity gives rise to a complicated classification for amphiboles (Hawthorne et al., 2012). Owing to the complexity, amphiboles are capable of accommodating a variety of elements with variable ionic charges and radii, including alkali elements, rare earth elements (REE), high field strength elements (HFSE), and large ion lithophile elements (LILE) (Siegel et al., 2017). Therefore, amphiboles are sensitive to chemical compositions of the crystallizing melts and may record some processes during magma evolution.

The Huangyangshan A-type granite located in the Kalamaili metallogenic belt, Xinjiang, is alkaline and contains abundant mafic microgranular enclaves (MMEs) (Yang et al., 2011). The reported ages for both units were 311–305 Ma and 300 ± 6 Ma, respectively (Su et al., 2008; Yang et al., 2011). The consistent ages along with the gradational contact between the host granite and MMEs and the presence of acicular apatite indicate magma mixing during the formation of the Huangyangshan A-type granite (Yang et al., 2009, 2010, 2011). In both units, Na-rich amphiboles are a common mineral phase. Therefore, in this paper, we choose amphiboles from the MMEs and their host granite to explore the compositional variations during magma mixing. Also, due to their sensitivity, amphiboles are potential geo-thermometer and barometer. For this reason, we tested whether they could yield proper estimates on the crystallization temperature and pressure of the amphiboles in the Huangyangshan A-type granite.

GEOLOGICAL SETTING

The Huangyangshan A-type granite, distributed along the Kalamaili thrust fault, is situated in the central part of the Kalamaili region in East Junggar, Xinjiang (**Figure 1**). This region represents the northern margin of East Junggar, part of the Junggar terrane that belongs to the Central Asian Orogenic Belt (CAOB) (Sengor et al., 1993; Xiao et al., 2003). The NW-SE trending Huangyangshan A-type granite covers an area of ∼230 km^2 and is intruded into the early Carboniferous strata, showing sharp contact (Yang et al., 2011). Contact metamorphism has also been observed, which implies shallow depth for emplacement (Yang et al., 2011). The granites consist of 40–55% alkali-feldspar, 5–15% plagioclase, 20–30% quartz, 5–10% mafic minerals (biotite and/or amphibole) and accessory minerals (< 1%) including apatite, zircon, and fluorite. Based on the content of mafic minerals, four main phases can be distinguished. A great number of MMEs with variable sizes are present in the granite. The MMEs exhibit sharp to diffuse contact with their host granite and chilled margins or biotite-rich reaction rims are locally present (**Figure 2**), indicating hybridization between MMEs and host granites (e.g., Yang et al., 2010). These MMEs are dioritic in composition and composed of 5–15% amphibole, 20–30% alkali-feldspar, 30–40% plagioclase, 5% biotite, and < 1% acicular apatite.

The Kalamaili region defines an important metallogenic belt in the East Junggar terrane. According to previous studies, Au and Cu mineralization are mainly distributed at the margins of calcic-alkaline granitoids, whereas tin mineralization mainly occurs at the margins of alkaline granitoids including the Huangyangshan granite (Yang et al., 2011).

ANALYTICAL METHODS

Petrographic and Electron-Microprobe Analyses

Doubly polished thin sections were made for rock samples collected from the Huangyangshan granite and the hosted MMEs. Petrographic observations were performed using optical microscopy and scanning electron microscope (SEM). All polished thin sections were carbon-coated and major element contents of amphiboles were determined using a JEOL JXA-8100 electron microprobe (Tokyo, Japan) at the Laboratory of Mineralization and Dynamics, Chang'an University. During EPMA analysis, the accelerating voltage, sample current, and beam diameter were 15 kV, 10 nA, and 5 μm, respectively. Fourteen elements in total were analyzed. The standards for calibrating element contents include: synthetic $MnTiO_3$ (for Mn Kα), plagioclase (Na Kα, Ca Kα, and Al Kα), magnetite (Fe Kα), sanidine (K Kα), zirconium metal (Zr Lα), olivine (Mg Kα and Si Kα), synthetic Nb-Ta alloy (Nb Lα and Ta Lα), synthetic rutile (Ti Kα), and fluorite (F Kα). The analytical precision (expressed as relative standard deviation) for major element oxide contents > 1 wt.% are better than 3%. Summary of EPMA data for amphiboles is given in **Table 1** and the complete EPMA dataset for amphiboles is presented in **Supplementary Material S1**.

Laser-Ablation ICP-MS Analysis

Trace elements of amphiboles were analyzed using a Photon Machines 193 nm excimer laser ablation system coupled with an Agilent 7700 ICP-MS (Santa Clara, CA, United States) at the Laboratory of Mineralization and Dynamics, Chang'an University. The analyzed elemental isotopes included ^{7}Li, ^{27}Al, ^{29}Si, ^{35}Cl, ^{45}Sc, ^{49}Ti, ^{55}Mn, ^{63}Cu, ^{66}Zn, ^{69}Ga, ^{85}Rb, ^{88}Sr, ^{89}Y, ^{90}Zr, ^{93}Nb, ^{118}Sn, ^{137}Ba, ^{139}La, ^{140}Ce, ^{141}Pr, ^{146}Nd, ^{147}Sm, ^{153}Eu, ^{157}Gd, ^{159}Tb, ^{163}Dy, ^{165}Ho, ^{166}Er, ^{169}Tm, ^{172}Yb, ^{175}Lu, ^{177}Hf, ^{181}Ta, ^{206}Pb, ^{232}Th, and ^{238}U. Helium gas was used as the carrier gas. The diameter, energy density, and repetition rate of the laser beam were 35 μm, 5.9 J/cm^2, and 8 Hz, respectively. For each analysis, signals on the gas background and samples or standards were collected for 10 s and 40 s, respectively. NIST SRM 610 and NIST SRM 612 were used as

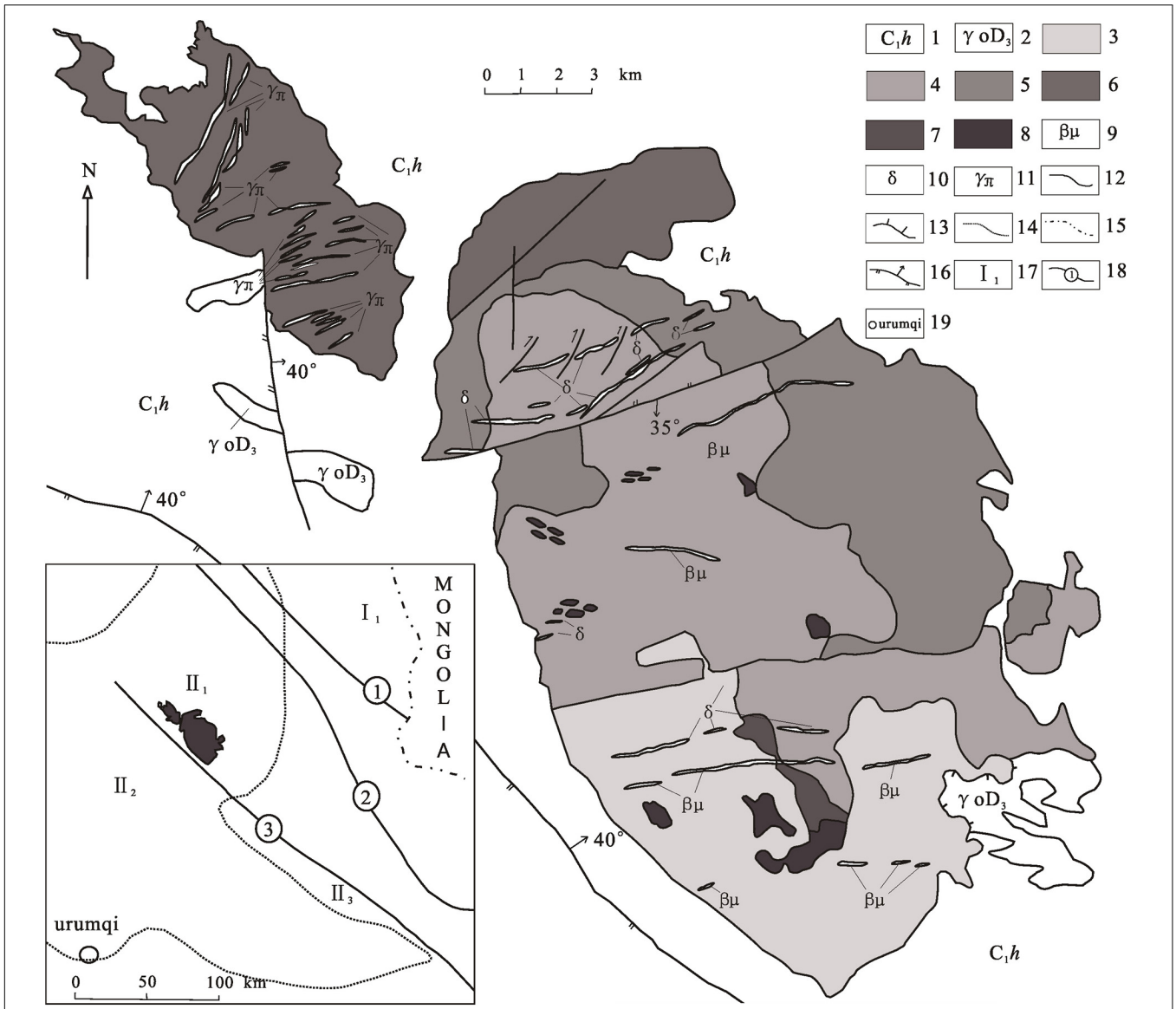

FIGURE 1 | Geological map of the Huangyangshan pluton (adapted from Yang et al., 2011). 1-Heshanshitou Group; 2-plagioclase granite; 3-medium grained biotite alkali feldspar granite; 4-medium grained hornblende alkali feldspar granite; 5-medium grained arfvedsonite alkali feldspar granite; 6-medium to fine grained arfvedsonite alkali feldspar granite; 7-fine grained biotite alkali feldspar granite; 8-fine grained mixed granite; 9-diabase dyke; 10-diorite dyke; 11-granite porphyry dyke; 12-pulsating contact; 13-beveling contact; 14-intrusive contact; 15-structural belt boundary; 16-fault and occurrence; 17 and 18-number of structure belt; I_1-Altai structure belt; I_2-Almantai structure belt; II_1-Kalamali structure belt; II_2-Junggar Basin; II_3-Jiangjunmiao structure belt: ① Irtysh Fault; ② Almantai Fault; ③ Kalamaili Fault.

the primary and secondary external standards, respectively. The LA-ICP-MS data were processed using Iolite v.3.71 (Paton et al., 2011) and the Si concentrations of the amphiboles obtained by EMPA was the internal standard for calculating trace element concentrations. The accuracy based on the test on NIST SRM 612 (expressed as relative difference between measured and reference values) was < 15% for most analyzed elements. The precision test on NIST SRM 612 indicated that the precision (expressed as relative standard deviation) was better than 10% for most analyzed elements except for Ti that showed analytical precision of 15.6%. The results are summarized in **Table 2** and the complete dataset of trace element concentrations is provided in **Supplementary Material S2**.

RESULTS

Petrography

The granite mainly exhibits medium- to fine-grained texture and vermicular texture and mantling texture are locally present. The major rock-forming minerals are alkaline feldspar (mainly perthite) and quartz, with minor plagioclase (An23 to An29,

FIGURE 2 | Field photos of the enclaves in the Huangyangshan alkaline granite. **(a–c)** Both sharp and transitional boundaries exist indicating the rheology of magma during magma mixing. **(d)** Alkali feldspar of the host granites crosscuts the boundaries of the MME.

TABLE 1 | Major element contents of amphiboles from the host granite and enclaves.

Amphibole	Granite Mean (n = 13)	Enclaves Mean (n = 2)	Amphibole	Granite Mean (n = 13)	Enclaves Mean (n = 2)
Na_2O	7.00	9.17	Al^{3+}	0.16	0.05
FeO	31.11	27.07	Fe^{3+}	0.14	0.03
K_2O	1.44	0.38	Mn^{2+}	0.05	0.04
F	0.79	0.27	Fe^{2+}	4.17	3.64
MnO	0.35	0.30	Mg^{2+}	0.04	0.16
CaO	3.00	4.86	*C-site*	4.75	4.11
SiO_2	48.83	50.90	Mn^{2+}	0.00	-
Ta_2O_5	0.04	0.04	Fe^{2+}	0.00	-
ZrO_2	0.07	0.57	Ca^{2+}	0.54	0.84
Al_2O_3	1.11	0.25	Na^{+}	1.45	1.16
SnO_2	0.00	0.01	*B-site*	2.00	2.00
MgO	0.16	0.65	Na^{+}	0.79	1.72
Nb_2O_5	0.01	0.03	K^{+}	0.30	0.08
TiO_2	1.63	1.26	*A-site*	1.09	1.80
Total	95.47	95.76	OH^{-}	1.09	1.56
Si	8.08	8.24	F^{-}	0.53	0.14
Al	0.05	–	O^{2-}	0.37	0.30
T-site	8.15	8.24	W-site	2.00	2.00
Ti	0.18	0.15	Fe#	0.97	0.99
Zr	0.01	0.05			

Fe# = $Fe^{3+}/(Fe^{2+} + Fe^{3+})$. The apfu values are calculated based on 24 oxygen atoms.

TABLE 2 | Average trace element concentrations (in ppm) of the amphiboles from the host granite and MMEs.

Comment	Granite		Enclaves	
	Core Mean (*n* = 7)	Rim Mean (*n* = 8)	Core Mean (*n* = 2)	Rim Mean (*n* = 4)
Li	1627.0	1375.1	480.8	1155.7
Al	6758.7	7339.8	1621.3	1802.0
Cl	7795.7	762.8	2122.9	4466.3
Sc	8.3	13.2	13.4	7.8
Ti	10054.3	7797.8	7177.9	8312.5
Mn	3007.1	2767.4	2395.9	3183.1
Cu	18.8	8.6	20.0	48.7
Zn	3153.1	2611.0	1129.6	1774.4
Ga	10.4	11.0	4.9	3.8
Rb	16.3	15.5	4.5	28.7
Sr	30.3	14.9	28.6	42.4
Y	169.8	81.8	346.8	278.9
Zr	461.7	364.1	4154.1	2843.7
Nb	74.5	36.4	20.7	65.4
Sn	14.3	9.2	39.8	35.7
Ba	2.7	2.9	2.2	3.9
La	18.9	13.0	22.5	12.6
Ce	58.5	46.6	172.6	79.4
Pr	10.3	8.3	14.8	7.7
Nd	53.8	43.3	82.9	38.7
Sm	16.7	12.7	31.4	14.3
Eu	0.1	0.1	0.3	0.2
Gd	16.5	11.0	38.6	19.8
Tb	2.6	1.8	7.1	4.0
Dy	17.3	11.8	49.6	31.3
Ho	4.7	3.3	12.3	8.7
Er	21.4	15.8	44.6	36.5
Tm	5.6	4.3	9.2	8.1
Yb	64.1	48.4	80.2	71.6
Lu	13.8	10.8	14.4	12.7
Hf	15.3	13.6	113.7	73.3
Ta	0.9	0.6	0.6	1.6
Pb	17.9	25.1	17.3	17.8
Th	0.9	0.4	4.7	1.9
U	0.5	0.5	2.2	1.6

b.d, represent the element content is below detection limit.

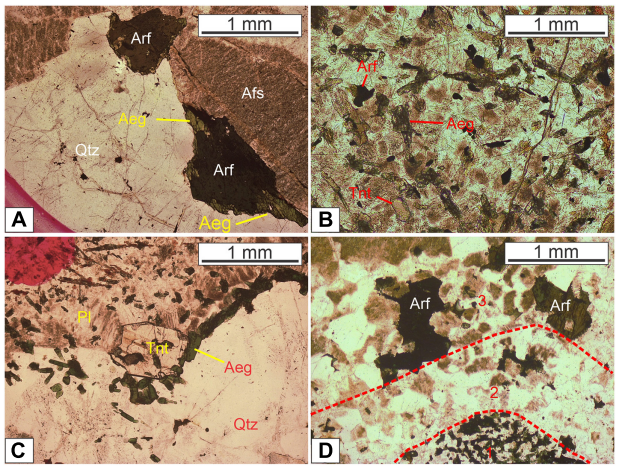

FIGURE 3 | Thin section photomicrographs showing **(A)** mantling texture in the granite; **(B)** titanite in MMEs; **(C)** mantling texture in the MMEs; **(D)** transitional boundary (1-Fine to microgranular enclaves; 2-Transition zone between granite and enclaves; 3-Medium grained arfvedsonite alkali feldspar granite). Mineral abbreviations: Qtz-quartz, Pl-plagioclase, Afs-alkali feldspar, Arf-arfvedsonite, Ae-aegirine, and Tnt- titanite.

oligoclase), biotite, and arfvedsonite (**Figure 3A**). Most aegirine occurs along the boundaries of amphibole grains in the host granite, indicating that arfvedsonite crystallize earlier than aegirine (**Figure 3A**), which may also imply the magma evolved toward more oxidized trend (Scaillet and MacDonald, 2001). The accessory minerals mainly include zircon, fluorite, and apatite. The presence of fluorite indicates that the granitic magma is likely F-saturated.

The MMEs mainly show subhedral granular texture and porphyritic texture and mantling texture locally occurs. Compared with the granite, the MMEs contain relatively abundant plagioclase and mafic minerals (mainly alkaline amphibole and aegirine), whereas the amounts of quartz and alkali feldspar are less than those of the host granite. The accessory minerals in the MMEs include titanite, apatite, and zircon. Apatite shows an acicular habit (**Figure 3B**), indicating a quench process. The amphibole crystallizes in a shape with excessively long *c*-axis and is semi-oriented (**Figures 3B,C**), suggesting that MMEs remained their rheology to some extent during formation. Typical transitional zone (diffuse contact) between the MMEs and the host granite can be observed under microscope (**Figure 3D**). It is also noted that quartz is mantled by a mineral assemblage consisting of aegirine and titanite (**Figures 3C**, **4a,b**). This texture is similar to quartz ocellus texture described in previous studies (e.g., Baxter and Feely, 2002; Renna et al., 2006). Back-scattered electron imaging shows that the early arfvedsonite is enclosed by the aegirine rimming the quartz xenocryst (**Figure 4b**). The replacement of arfvedsonite by aegirine can also be observed (**Figure 4c**), indicating that the aegirine postdates the arfvedsonite. Other mafic minerals including biotite are only present in minor quantities. Zircon as an accessory phase is often subject to hydrothermal alteration (**Figure 4d**).

Major Element Compositions of Amphiboles and Formula Assignments

The average major and trace element compositions of amphiboles are given in **Tables 1**, **2**, respectively. Major and trace element compositions of the host granite and MMEs from Su et al. (2008) and Yang et al. (2011) are also listed in **Table 3** for comparison (complete dataset of bulk rock is given in **Supplementary Materials S3, S4**).

The K content of amphiboles from the host granites ranges from 0.275 to 0.371 apfu and shows a dichotomy that one group exhibits higher value (0.352–0.371 apfu) whereas the other lies

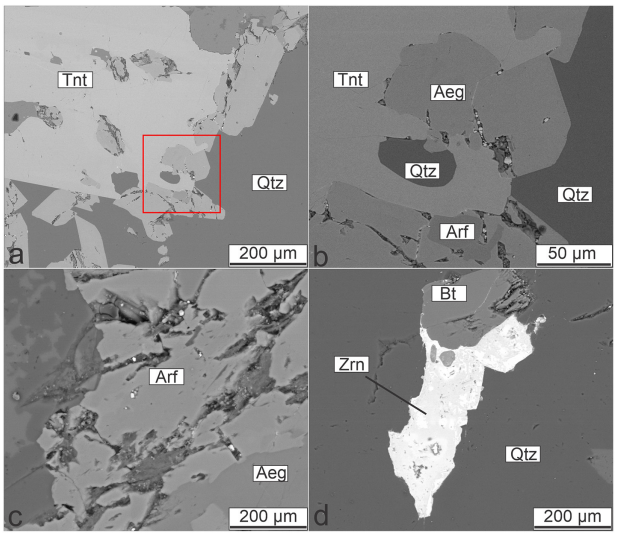

FIGURE 4 | Backscattered electron (BSE) images showing typical textures in the MMEs. **(a)** BSE image of the mantling texture showed in **Figure 3C**. **(b)** Enlargement of the area in the red box in **(a)**. **(c)** Replacement of arfvedsonite by aegirine. **(d)** Zircon associated with biotite and quartz.

below the median value (∼ 0.3125 apfu), ranging from 0.215 to 0.304 apfu. The K content of amphiboles from the MMEs lies in the above-mentioned two ranges respectively. The Na content of amphiboles from both the granite and MMEs vary in a narrow range (2.185–2.488 apfu) except two analyses showing abnormally low values. The Ca content of amphibole from the host granite ranges from 0.235–0.607 apfu except one analysis showing abnormally high value (1.039 apfu), whereas the Ca content of amphibole from the MMEs is relatively low (∼ 0.25 apfu). The Mg, Si and Mn^{2+} show similar patterns that the amphibole from granites have constrained Mg, Si and Mn^{2+} in relatively low values (0.004–0.120 apfu, 7.81–8.351 apfu, 0.043–0.054 apfu, respectively) whereas the amphibole from the MMEs have higher Mg, Si and Mn^{2+} (∼0.6 apfu, ∼8.3 apfu, ∼0.075 apfu, respectively). Ti and Al show opposite patterns that amphiboles of granites (0.187–0.214 apfu, 0.064–0.409 apfu, respectively) have higher Ti and Al than MME-host amphiboles (0.017–0.211 apfu, 0.044–0.084 apfu, respectively). Fe^{3+} is calculated based on algorithm provided by Locock (2014) and both granite-host and MME-host amphiboles share a similar range of Fe^{3+} (0–0.620 apfu) and Fe^{2+} (3.669–4.423 apfu). Fluorine content ranges from 0.2–0.9 apfu and Cl content is below 0.1 apfu except HY5-9 which has 1.4 apfu Cl. The abnormally high value of HY5-9 may be ascribed to Cl-rich inclusions.

After analyzing the major elements of amphiboles, the chemical formula of amphibole can be calculated. Generally, the amphiboles-group minerals have a structure formula as $AB_2C_5T_8O_{22}W_2$, and the specific formula can be calculated using the spreadsheet provided by Locock (2014). The results of the formula assignment are listed in **Table 4** (the detailed formulae assignment is given in **Supplementary Material S5**). In our case, the A-site of amphiboles is occupied by Na^+, K^+ and vacancies;

TABLE 3 | Average whole-rock major and trace element contents of the host granite and MMEs.

Unit	Host granite	MMEs
Samples	**(n = 18)**	**(n = 2)**
SiO_2 wt%	75.9	58.8
TiO_2	0.3	1.0
Al_2O_3	11.0	16.2
TFe_2O_3	2.6	7.2
MnO	0.1	0.1
MgO	0.1	2.7
CaO	0.5	3.7
Na_2O	3.8	6.0
K_2O	4.3	3.2
P_2O_5	0.1	0.2
LOI	0.5	0.5
Total	98.8	99.2
Li (ppm)	107.36	114.01
Be	5.08	1.96
Sc	3.13	14.88
V	1.05	141.43
Cr	21.03	22.59
Co	0.20	18.11
Ni	8.32	11.41
Cu	2.25	5.57
Zn	73.26	137.40
Ga	24.22	21.34
Rb	173.44	92.28
Sr	34.33	246.80
Y	68.16	48.80
Zr	341.49	166.07
Nb	14.50	10.46
Mo	0.60	0.28
Cd	0.17	0.14
In	0.22	0.17
Cs	13.05	12.68
Ba	100.73	314.72
La	31.15	23.04
Ce	69.13	53.50
Pr	9.46	7.54
Nd	38.21	31.40
Sm	9.56	7.43
Eu	0.21	1.04
Gd	10.29	7.45
Tb	1.92	1.34
Dy	11.64	8.26
Ho	2.49	1.70
Er	7.27	5.07
Tm	1.20	0.80
Yb	7.86	5.28
Lu	1.14	0.74
Hf	11.25	5.17
Ta	1.49	1.39
Pb	24.51	16.69
Bi	0.70	0.29
Th	13.78	9.49
U	4.60	2.92

The whole-rock geochemical data are cited from Tang et al. (2007), Su et al. (2008), and Yang et al. (2010).

TABLE 4 | Average calculated formulae and cation assignments (in apfu) of amphiboles based on (Locock, 2014).

Unit	Amphibole/granite	Amphibole/MMEs
Samples	**(n = 12)**	**(n = 2)**
T-site (8)	8.17	8.32
Si	8.14	8.32
Al^T	0.03	0.00
C-site (5)	4.79	4.68
Ti^C	0.20	0.11
Al^C	0.18	0.06
Zr	0.01	0.00
Mn^{2+}	0.05	0.07
Fe^{3+}	0.15	0.12
Fe^{2+}	4.17	3.96
Mg	0.04	0.34
B-site (2)	2.00	2.00
Na^B	1.56	1.75
Ca	0.44	0.25
A-site (1)	1.00	0.92
Na^A	0.70	0.60
K	0.30	0.32
W-site (2)		
F	0.41	0.56

The ideal number of each site is given in the brackets.

B-site is occupied by Na^+ and Ca^{2+}. In both sites, Na^+ is the dominant cation. Therefore, these amphiboles belong to sodic amphiboles enriched in alkali. The octahedral C-site is occupied by various cations Ti^{4+}, Al^{3+}, Zr^{4+}, REE^{3+}, Mg^{2+}, Fe^{2+}, Fe^{3+}, Mn^{2+}, etc. The tetrahedral T-site is dominated by Si^{4+} with less Al^{3+}. The W-site mainly contains anions F^-, Cl^- and OH^-, indicating ^{W}(OH, F, Cl)-dominant amphiboles. According to the formula, W-site also contains O^{2-}, the amount of which is calculated by Ti in apfu (Oberti et al., 1992).

In **Table 4**, The C-site often shows low occupancy (< 5 apfu), whereas the A-site has an over-occupancy (> 1 apfu), although the average value seems to be in the normal range. The low occupancy of the C-site and over-occupancy of the A-site cannot be reduced, no matter how we changed calculation procedures and normalization schemes or set up different initial Fe^{2+}/Fe^{3+} ratios and oxo-components. However, this issue seems to be common for alkali amphiboles in alkaline and peralkaline rocks, as reported by Hawthorne et al. (1993). The reason may be related to the misfit of B-site cations in C-site that is followed by A-site cations shifting to B-site (Siegel et al., 2017). Although cation misfit may exist, B-site cations, which determine the sub-group of amphiboles, do not show such shift in formula and still point out that most amphiboles from the Huangyangshan granite and MMEs are sodic amphiboles.

Trace Element Chemistry of Amphiboles

The chondrite-normalized amphiboles REE pattern of both MMEs and granites are generally similar (**Figures 5E,F**), characterized by relatively flat light and middle REE, marked negative Eu-anomaly and an enrichment in HREE (**Figures 5B,D**). The $(La/Sm)_N$, Eu/Eu* and $(La/Yb)_N$ of amphiboles range from 0.42–1.74, 0.004–0.028, 0.03–0.13 in MMEs and 0.45–1.43, 0.002–0.039, 0.03–0.73 in granites. Amphiboles REE pattern of MMEs shows a weakly positive Ce-anomaly (1.19–1.63) with slightly lower total REE concentration than that of amphiboles hosted in granites (**Figure 5D**). The abundance of REE in each amphibole varies significantly, nearly an order of magnitude.

The primitive mantle-normalized trace elements pattern of amphiboles shows a negative Ba, Eu, Sr anomalies and positive Pb anomaly (**Figures 5A,C**). The Ba, Sr, Pb contents of amphiboles range from 1.61–6.40 ppm, 18.45–90.10 ppm, 9.06–25.60 ppm in MMEs and 0.45–11.50 ppm, 3.43–150.60 ppm, 7.54–58.60 ppm in granites. In amphiboles of MMEs, Nb and Ta show a positive anomaly compared with adjacent U, Th and La, Ce (**Figures 5A,C**). Nb, Ta, U and Th contents of amphiboles range from 8.62–150.10 ppm, 0.68–5.94 ppm, 0.03–1.22 ppm and 0.08–2.69 ppm, respectively. Zr and Hf of amphiboles do not show noticeably anomaly both in MMEs and granites but with an enrichment of Hf compared with Zr. The Zr and Hf concentrations of amphiboles range from 19.4–494.00 ppm, 1.19–49.30 ppm in MMEs and 161.00–728.00 ppm, 5.50–27.10 ppm in granites. These trace elements plotted in the spidergram also vary significantly.

Compared with the bulk compositions of the granite and MMEs, the Nb and HREE concentrations of the amphiboles are higher than the whole-rock Nb and REE concentrations (**Tables 2**, **3**), whereas the LILE, Th, U and LREE concentrations of the amphiboles are lower, implying that HREE and Nb are more compatible in amphiboles than LILE, Th, U and LREE.

DISCUSSION

Magma Mixing and Formation of MMEs in the Huangyangshan Granite

Petrogenesis of MMEs and A-type granites are still controversial because of their complex geochemical characteristics (Bonin, 2007). MMEs are commonly found in granitoids and are more mafic than their host rocks in chemical compositions. Due to the compositional difference and the occurrence of MMEs, the MMEs was first regarded as refractory residues of partial melting and entrained by granitoids (White and Chappell, 1977). To date, four hypotheses have been proposed to explain the genesis of MMEs:

1) Refractory residues of partial melting source (e.g., White and Chappell, 1977; Barbarin and Didier, 1992; White et al., 1999; Chappell et al., 2000);
2) Early cumulus from host magma (e.g., Dodge and Kistler, 1990; Chen et al., 2009; Shellnutt et al., 2010; Huang et al., 2014);
3) Xenolith of wall rocks captured by magma (e.g., Yang et al., 2004, 2006);
4) Magma mixing through mafic magma injected into chambers of less mafic magma (e.g., Wiebe et al., 1997; Kumar and Rino, 2006; Su et al., 2008; Guo et al., 2010; Yang et al., 2010, 2011).

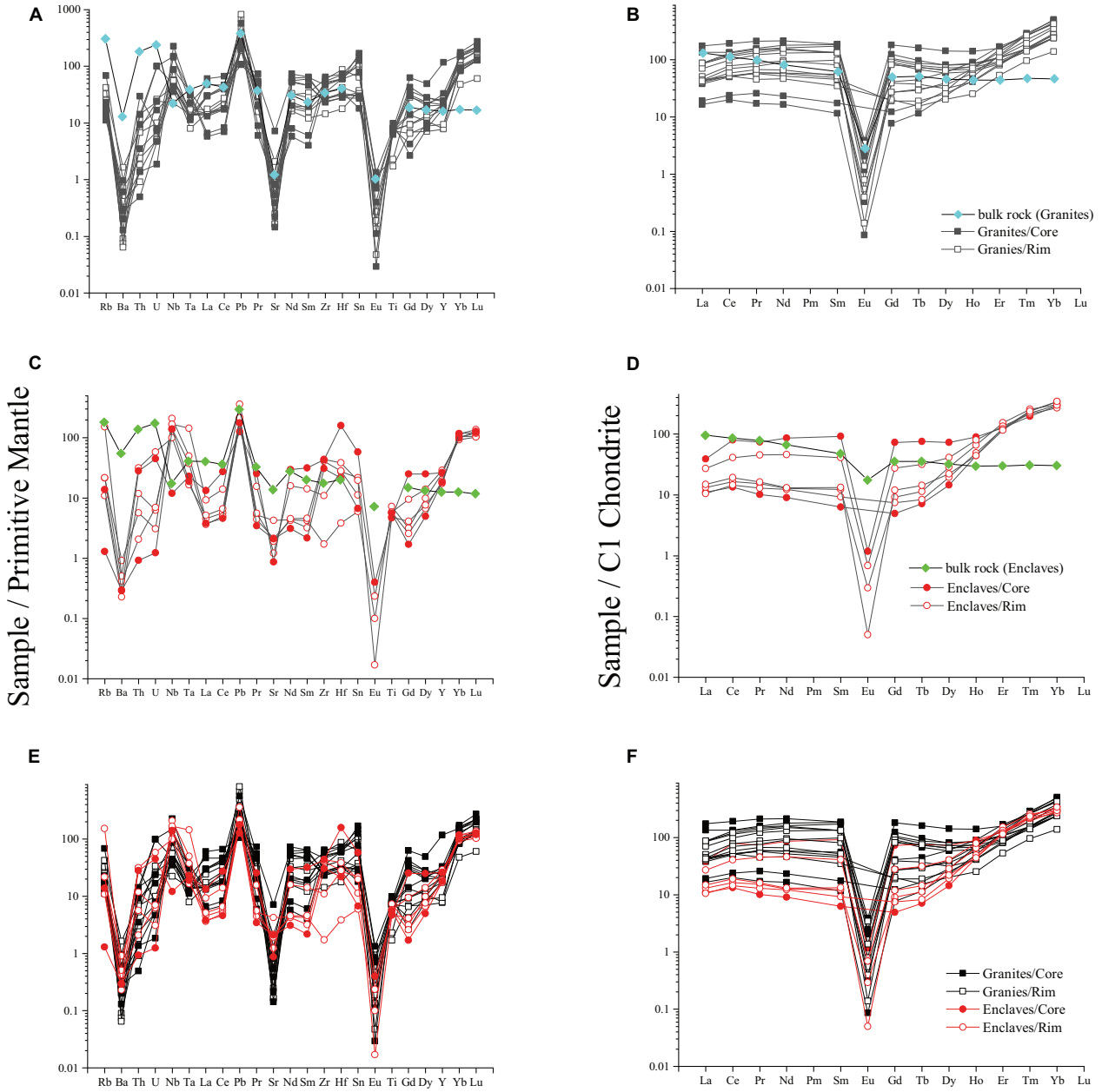

FIGURE 5 | Chondrite-normalized REE and primitive mantle-normalized trace element profiles of the amphiboles from gantries and MMEs and average bulk rock profiles of the hosts. **(A)** REE and **(B)** trace element spider diagram for the granites and their amphiboles; **(C)** REE and **(D)** trace element spider diagram for the MMEs and their amphiboles; **(E)** REE and **(F)** trace element spider diagram show contrasting between amphiboles of granites and MMEs and between cores and rims of amphiboles. The chondrite values and primitive values are from Sun and McDonough (1989).

5) Different crust-derived melts mixing (e.g., Roberts and Clemens, 1993; Domanska-Siuda et al., 2019).

Although the petrogenesis of MMEs is still open to debate, the magma mixing model is the most widely accepted. The mixing processes provide constraints on the petrogenesis and sources of granitoids and information about the tectonics settings (Yang et al., 2006, 2011; Kazemi et al., 2019).

In our case, major and trace elements of the MMEs and granites prove that the MMEs formed via magma mixing (**Figure 6**). If we assume mafic magma similar to the average oceanic crust injected into the average host granites that are little influenced by the mafic magma, this two end-members mixing in **Figure 6B** shows that nearly 40-70% of felsic magma added to the mafic magma. Besides, zircon U-Pb ages support magma mixing because both MMEs and host granites are contemporary and the acicular apatites resulted

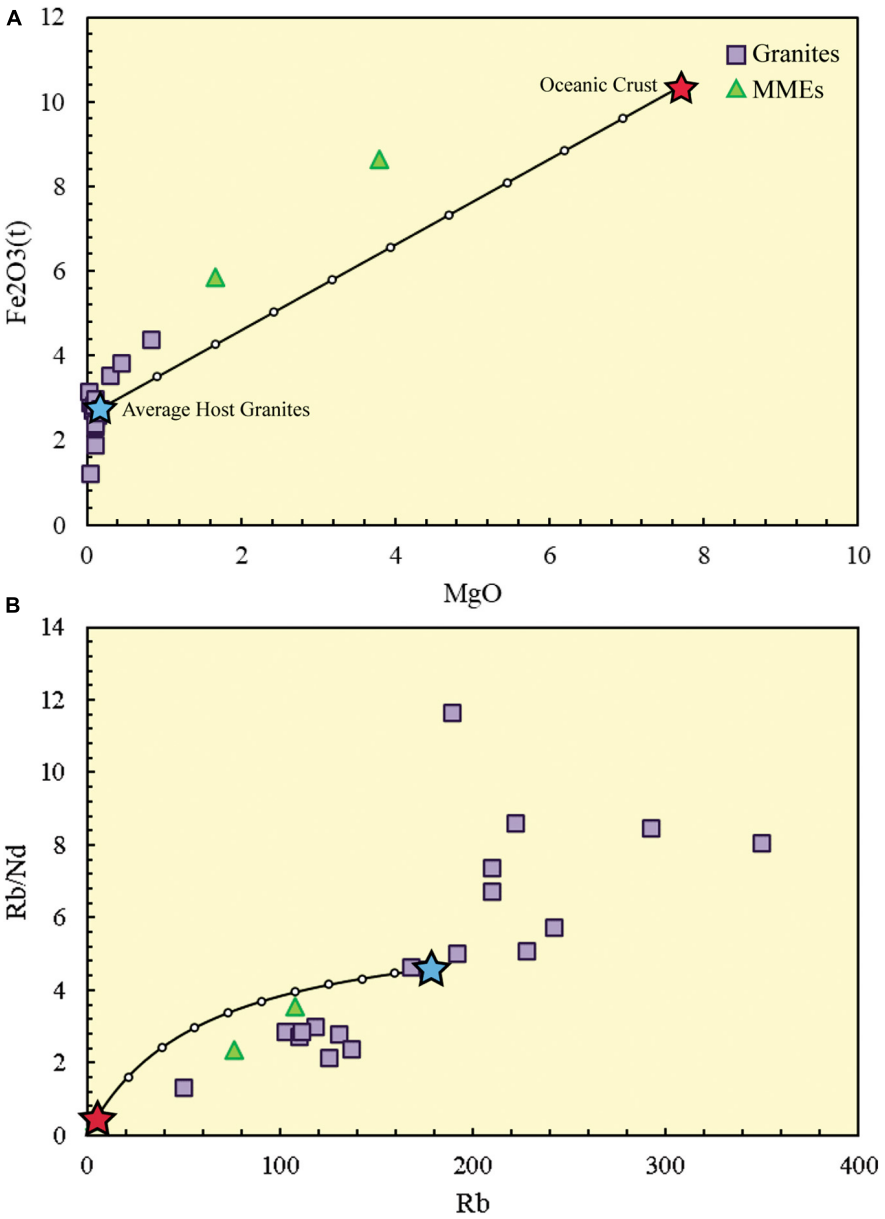

FIGURE 6 | Binary plots with magma mixing curves. **(A)** MgO versus Fe_2O_3 (Zorpi et al., 1989); **(B)** Rb/Nd-Rb (Schiano et al., 2010). The estimation shows that ~40-70% felsic magma mixed with mafic magma.

from quenching hot mafic magma within cold felsic magma (Yang et al., 2011).

Voluminous felsic magma contaminated the mafic magma rendering the trace elements pattern of the MMEs resembles that of host granites. Therefore, as a late phase, amphiboles from both units are depleted in Ba, Eu, Sr while enriched in Pb. The similar patterns of REE and other trace elements reflect homogeneous mixing in trace elements which is also supported by the absence of zonation of amphiboles. In contrast, the major element contents are not only under control of the magma composition but are also influenced by other factors like crystal structure and valence balance. Therefore, the major elements of both amphiboles should record the chemical variation during magma mixing.

Compositional Variation of Amphiboles

Halogens in W-Site of Amphiboles

A-type granites and their sodic amphiboles are usually enriched in halogens such as F and Cl. As W-site anions, F^- and Cl^- can substitute for OH^- and O^{2-} (Hawthorne et al., 2012). Substitution between $(F^-, OH^-, Cl)^-$ and O^{2-} require involvement of Ti^{4+} to maintain charge balance, i.e. $(Mg, Fe)^{2+} + 2\ (OH, F, Cl)^- \rightarrow Ti^{4+} + 2\ O^{2-}$ (Oberti et al., 1992). Therefore, if F and Cl contents are controlled by crystal

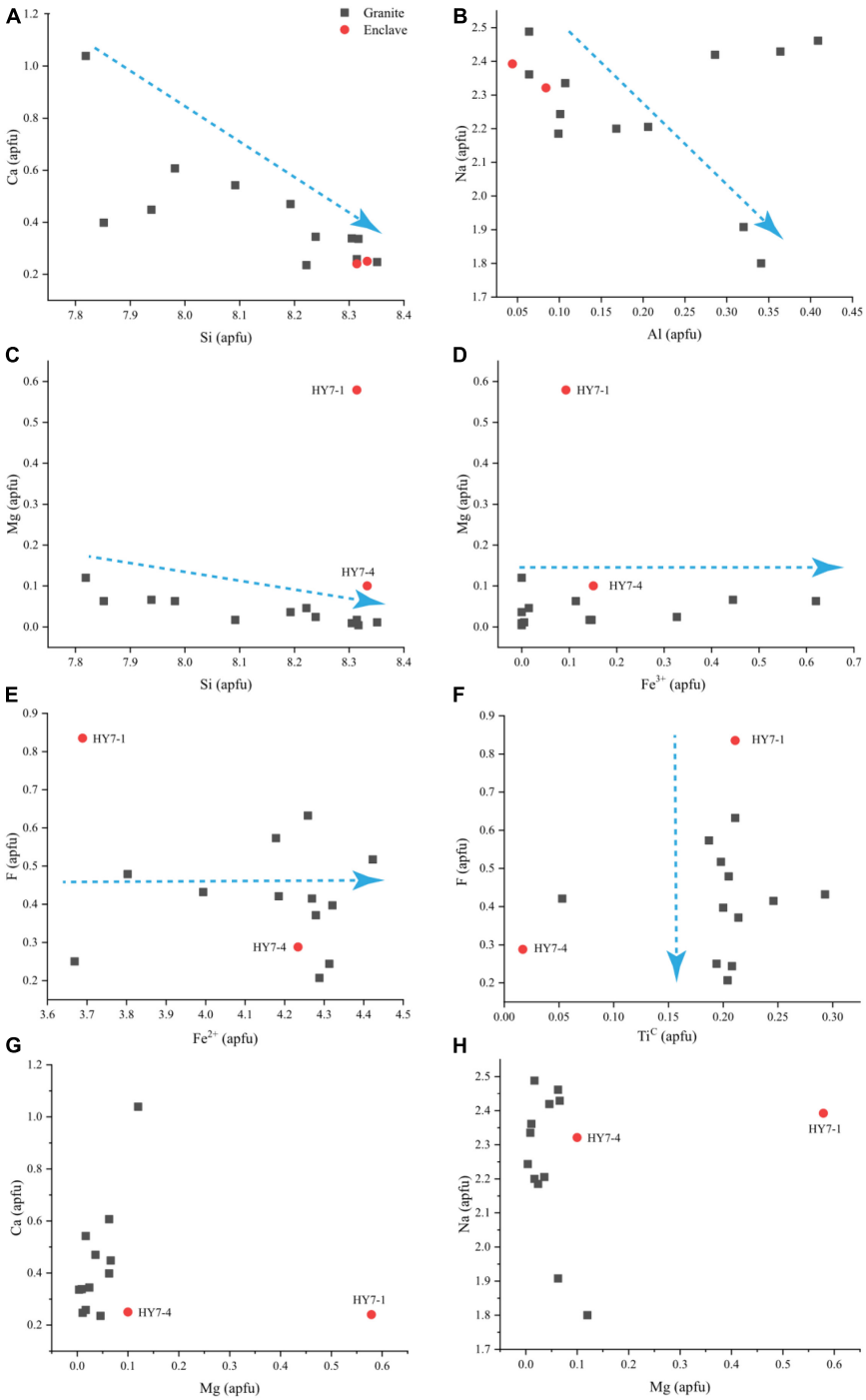

FIGURE 7 | Binary diagrams showing major elements concentrations of amphiboles in atoms per formula unit (apfu). **(A)** Ca versus Si; **(B)** Na versus Al; **(C)** Mg versus Si; **(D)** Mg versus Fe^{3+}; **(E)** F versus Fe^{2+}; **(F)** F versus Ti in C-site; **(G)** Ca versus Mg; and **(H)** Na versus Mg. In the plots, black squares represent chemical composition of granites-host amphiboles, red circles represent chemical composition of enclave-host amphiboles.

chemistry, they must show a negative correlation with Ti. However, **Figure 7F** shows that Ti in the amphiboles has no clear correlation with F and Cl, implying that F in the amphiboles is mainly influenced by chemical compositions of host rocks, other than crystal chemistry. Similarly, F and Cl do not show correlation with Fe (**Figure 7E**), implying that the influence of Fe-F avoidance principle (e.g., Morrison, 1991) is negligible and also supporting the conclusion that halogens are mainly controlled by chemical compositions of melts.

Although amphiboles in our case crystallize as later phases, the variation of F still records the evolution of itself during

magma mixing. Because the chemical variation of magma is the only factor that influences F in the amphiboles, lower F content of amphiboles from F-saturated granites reflects that F decreased during evolution before magma mixing, which could be the result of fluorite crystallization. Subsequent mixing that the lowered the F content of the MMEs is recorded by the amphiboles from the MMEs.

Although crystal chemistry has little influence on F content, conversely, abundance of F can control partitioning of major and trace elements that occupies other sites and further cause change in crystal chemistry (Adam et al., 1993; Iveson et al., 2017, 2018). In aluminosilicate melts, elevated silica and alumina contents normally enhance polymerization whereas addition of F would form F-Si and F-Al complexes and depolymerize the melts (Iveson et al., 2017). In addition, polymerization of melts is a key factor that controls the partition coefficients of HFSE, REE and some other economic metals (e.g., Mo, W, Nb). Generally, the lower polymerization degree of the melt is, the lower $D^{amp/melt}$ of these elements will become (Iveson et al., 2018). On the contrary, Cl prefers to form alkali-Cl complexes, resulting in higher polymerization that facilitates incorporation of trace element into amphibole. In our case, both amphiboles from the host granites and MMEs are F-rich and Cl-poor, which is consistent with the conclusion that F is compatible in amphiboles and Cl is incompatible in amphiboles (e.g., Van den Bleeken and Koga, 2015). Although lacking reliable partition coefficients that are applicable for using amphibole halogen contents to estimate the halogen contents of the melts, the influence of halogens on major and trace elements partitioning cannot be ignored.

Can Cations of A-, B-, and C-Sites Trace Magma Mixing?

A- and B-sites are mainly occupied by Na with considerable K and Ca. On B-site, Na^+ and Ca^{2+} can substitute for each other, followed by T-site substitution between Si^{4+} and Al^{3+}. This coupled substitution can be expressed using the following reaction:

$$^{B}Na^{+} + {}^{T}Si^{4+} \leftrightarrow {}^{B}Ca^{2+} + {}^{T}Al^{3+}$$

Similarly, K^+ and Na^+ can also substitute for each other on A-site without any change in valence. For fluoro- sodic-amphiboles, elevated Na and F can constitute local configuration of ^{A}Na-^{W}F-^{B}Na to maintain the stability of amphiboles (Hawthorne et al., 1996).

In **Figures 7A,B**, negative correlations of Ca-Si and Na-Al reflect Ca and Na are under the control of substitution and thus B-site cations cannot trace chemical variation of magma. The substitution of B-site also influences the A-site and the sum of cations of A-site often exceed 1 apfu, indicating crystal chemistry dominates the behavior of K and Na^A (**Supplementary Table 5**).

Although the bulk CaO content of the MMEs is higher than the host granite (**Table 1**), the amphibole from the MMEs contain lower CaO content than that from the host granite. The reason for such discrepancy may be ascribed to MMEs containing more plagioclase than the granite. Therefore, more Ca partitions into plagioclase other than amphibole. Different from the CaO content, the Na_2O and K_2O contents of the amphiboles from both units are comparable, although the K_2O contents of the amphiboles are much lower than the bulk K_2O contents of both rock units. This phenomenon may be ascribed to Na having higher diffusivity than K and further imply the melt mixing cannot be fully traced by major elements of A-site either (Hawthorne et al., 2005).

As trace elements, Pb, U and Th can be incorporated into A- and B-site (Tiepolo et al., 2007; Hawthorne et al., 2012). Generally, Pb occupies the A-site, whereas U and Th occupy the B-site. Although they are expected to occur mostly as tetravalent cations which are unsuitable for A- and B-site from the perspective of charge balance, due to their small ionic radii, they prefer to occupy these sites in contrast (Tiepolo et al., 2007). Partitioning of Pb, U and Th is mainly controlled by melt compositions (i.e., polymerization of magmas). In addition, partitioning of U is also influenced by the redox state, because U^{6+} is difficult to incorporate into amphibole. In this study, the Pb contents of amphiboles is similar to their hosts, indicating Pb is not so incompatible. This is consistent with the results of Brenan et al. (1995) and Tiepolo et al. (2007). Uranium and Th also have higher partition coefficients in sodic amphiboles than calcic amphiboles (Tiepolo et al., 2007).

More interestingly, Li is commonly expected to substitute for Na. It can also replace cations such as Mg or Fe^{2+} via coupled substitution on C-site (e.g., Hawthorne et al., 1993, 1994; Oberti et al., 2003), which brings complexity in discerning the occupancy of Li.

Incorporation mechanism of Li in amphiboles includes (e.g., Hawthorne et al., 1994):

$$Li^{+} \leftrightarrow Na^{+}$$

$$Li^{+} + Fe^{3+} \leftrightarrow 2Fe^{2+} \text{or} 2Mg^{2+}$$

$$Si^{4+} + Li^{+} \leftrightarrow Al^{3+} + Mg^{2+}$$

$$Ca^{2+} + Li^{+} \leftrightarrow Na^{+} + Mg^{2+}$$

In our case, Si and Mg show a negative correlation, which indicates that C-site occupied by Li is coupled with Si incorporated in T-site (**Figure 7C**). This process may further explain why T-site shows excess Si (> 8 apfu).

Besides Li, the C-site of amphiboles is mainly occupied by Fe^{2+} and minor Mg^{2+}, Mn^{2+}, Ti^{4+} and Fe^{3+} (e.g., Hawthorne et al., 2012). Because Fe^{3+} and Fe^{2+} cannot be directly determined by EMPA, the content of Fe^{3+} is estimated through algorithm based on charge balance (Locock, 2014). Therefore, Fe^{3+}/Fe^{2+} cannot represent the redox state since no Mn^{3+} exists in the amphiboles. No correlation between Fe^{3+} and Mg^{2+} also supports this (**Figure 7D**). In our case, C-site is only partly filled (< 5 apfu), the effect of crystal chemistry is insignificant except for Al, which is allocated to both C- and T-site, the latter where Si constrain the behavior of Al. Although Si negatively correlates with Mg, implying the Li-substitution (**Figure 7C**), the

Li content of amphiboles is too low to significantly influence the variation of Mg. Also, considering amphibole is the major carrier of Mg in both MMEs and host granites, Mg in amphiboles records the evolution of magma. Therefore, the amphiboles of the MMEs and host granites prove that high MgO magma mixed with low MgO magma.

The variations of Fe and Ti of amphiboles are different from their hosts. As suggested by the mixing model, the unmixed mafic magma is higher in Fe and Ti than granites but Fe and Ti of amphiboles from the MMEs are lower than those of granites. If we assume the high MgO amphibole crystallized earlier than low MgO amphiboles, the former has lower Fe and higher Ti while the latter is opposite depicts such a scenario: when high-MgO amphibole crystallized, the crystallization of titanite and Fe-oxide had already decreased the Fe and Ti content of the mixed magma, as evidenced by the similar range of Ti content among high-MgO amphibole and amphiboles from granites; subsequent injection of felsic magma replenish the Fe to increase the Fe of low-MgO amphibole while consistently crystallizing titanite further lower the Ti of low-MgO amphibole.

Similar to Ti, other HFSE (including Nb, Ta, Zr, Hf) also occupy C-site but behave diversely. Zr^{4+} and Hf^{4+} have the same valence as Ti^{4+} but larger ionic radii (Shannon, 1976), Zr and Hf are thus sensitive to compositional change of amphiboles or melts (Tiepolo et al., 2007). In contrast, although Nb^{5+} and Ta^{5+} have higher valence and the high valence can be balanced by oxo-component introduced during Ti incorporation ($(Mg, Fe)^{2+} + 2(OH, F, Cl)^{-} \rightarrow Ti^{4+} + 2O^{2-}$) (Tiepolo et al., 2001, 2007). Hence, Nb and Ta in amphiboles could behave as slightly incompatible or even compatible elements with increasing Ti (Tiepolo et al., 2007). In both the Huangyangshan granite and its MMEs, Zr and Hf show different partitioning behavior between the amphibole and melt. Niobium is relatively compatible compared to Ta in the amphibole from the granite whereas both Nb and Ta behave compatibly in the amphibole from the MMEs (**Figures 5A,C**).

Distribution of REE

Distribution of REE in amphibole-group minerals is mainly influenced by crystal structure and melt compositions. The effect of melt compositions relates to major elements that are involved during incorporation of REE into amphiboles. The difference in substitution mechanism can be justified by different site preference between LREE and HREE (Bottazzi et al., 1999; Shimizu et al., 2017). Similarly, the size of different sites also controls the site preference of REE (Blundy and Wood, 1994). Many studies have demonstrated that LREE prefer to substitute for Ca^{2+} whereas HREE prefer to substitute for Fe^{2+} corresponding to M4-site (B-site) and M4'-site (B-site) or M2-site (C-site) respectively (e.g., Bottazzi et al., 1999; Tiepolo et al., 2007).

Due to the lower Ca content and higher Fe content of sodic amphibole, HREE are much more compatible than LREE in sodic amphibole and the $D_{amph-melt}$ of REE in our case are higher than the values reported in other studies (**Table 5**; e.g., Marks et al., 2004; Siegel et al., 2017). The REE partition coefficients of the amphibole from the host granites show a pattern that from La to Td and from Dy to Lu, each group fits a specific parabolic trend that can be calculated using the model of Blundy and Wood (1994). However, REE partition coefficients of the amphibole from the MMEs do not show the same trend but monotonically increase from La to Lu instead (**Figure 8**). This phenomenon may indicate that in melts with different compositions, site preference of REE could be different. In addition, the partition coefficients decrease from core to rim (**Table 5**; complete partition coefficients of REE between amphiboles and their hosts are given in **Supplementary Material S6**), regardless of the hosts of amphiboles, implying that most REE are distributed into accessory minerals, such as titanite and/or zircon.

Temperature and Pressure Estimate of Sodic Amphiboles

According to major and trace elements, zircon U-Pb ages, texture, and rheology, the petrogenesis of the MMEs hosted by the Huangyangshan A-type granite requires mafic magma injection (**Figure 9**). If the amphiboles are the later phase during magma mixing, they may record similar temperature. Notably, most thermometers and barometers for amphibole are based on chemical compositions of calcic amphiboles. However, in our case, amphiboles are mostly sodic amphiboles that may not be suitable for these thermometers and barometers (e.g., Ridolfi et al., 2010; Ridolfi and Renzulli, 2012; Putirka, 2016). Therefore, the prerequisite is to test whether these amphiboles have intrinsic flaws that prevent them from estimating temperature or pressure and seek for a reference value to test the estimates of various thermometers.

Before testing and estimating the crystallization temperatures of the amphiboles, an "amphibole-saturation temperature" for a given liquid composition can be estimated using liquid-only thermometer provided by Molina et al. (2015). Because the chemical compositions of amphiboles are not needed for calculation, liquid-only thermometer can yield reasonable values of 1024 ± 42℃ for MMEs and 843 ± 42℃ for granites, regardless of the species of amphiboles.

TABLE 5 | Apparent melt-amphiboles partition coefficients ($D_{Amp-bulk}$) of rare earth element (REE).

	$D_{core-granite}$	$D_{rim-granite}$	$D_{core-MMEs}$	$D_{rim-MMEs}$
La	0.39	0.59	0.17	0.26
Ce	0.63	0.83	0.26	0.53
Pr	0.82	1.07	0.28	0.53
Nd	1.06	1.39	0.31	0.71
Sm	1.25	1.73	0.39	1.01
Gd	0.99	1.56	0.39	1.07
Tb	0.87	1.34	0.46	1.16
Dy	0.96	1.46	0.86	1.34
Ho	1.28	1.86	1.99	2.23
Er	2.13	2.86	4.29	4.12
Tm	3.62	4.57	7.42	6.97
Yb	6.17	7.93	9.80	10.15
Lu	9.48	11.81	11.65	12.58

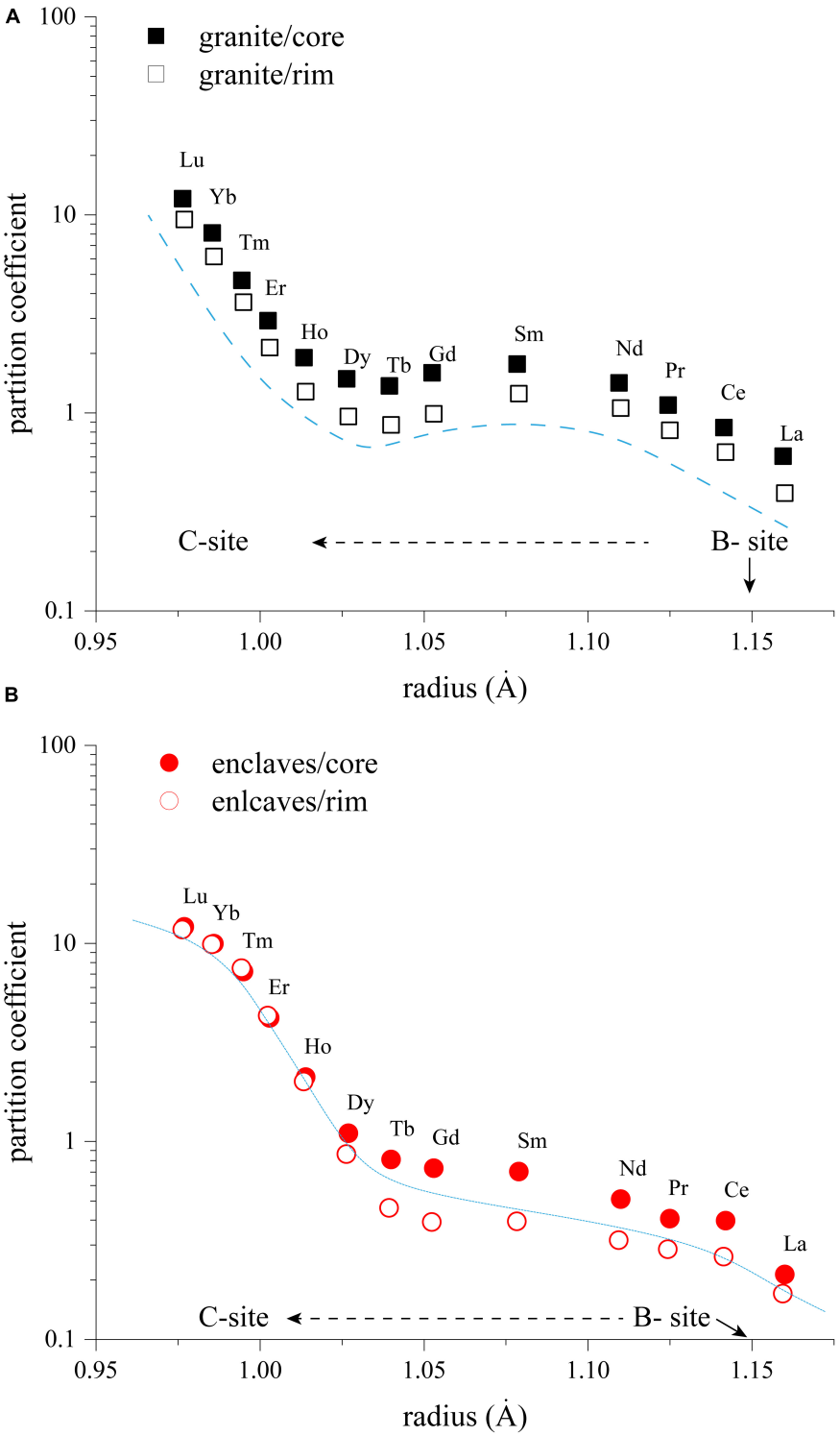

FIGURE 8 | Diagrams showing the relationship between ionic radii and apparent partition coefficient $D_{amph-melt}$ (average REE content of amphiboles/average REE content of the bulk rock) for amphiboles from the host granite **(A)** and from the enclaves **(B)**. Blue dash lines represent Lattice-Strain Theory fit through these data. Black dash lines reflect potential site preference of REE.

We then tested and estimated the crystallization temperatures of the amphiboles from the Huangyangshan granite and its MMEs using amphibole-only thermometers and thermometers based on partition coefficients. Amphibole-only thermometers are based on the correlation between temperature and chemical compositions of amphiboles that are either experimentally synthesized or natural samples (e.g., Ridolfi et al., 2010; Ridolfi and Renzulli, 2012; Putirka, 2016). Through these algorithms, the temperature estimates for the amphiboles in the MMEs and host granite are consistent within errors (∼ 650°C), implying that the amphiboles crystallize as late phase, consistent with the fluorite, titanite, and Fe-oxide crystallized earlier than amphiboles (Price et al., 1999; Scaillet and MacDonald, 2001). As for thermometers based on partition coefficients, Molina et al. (2015) and Putirka (2016) recommend thermometers derived from correlation between temperatures and D_{Mg} or D_{Na}. Although Molina et al. (2015) emphasized that their dataset only contained amphiboles with $Ca^B/(Ca^B + Na^B) > 0.75$, Mg in amphiboles does not show any correlation with Ca or Na in our case (**Figures 7G,H**), therefore the thermometer provided by Molina et al. (2015) may be applicable to our samples. The temperature estimates are 946 ± 45°C for amphiboles in the MMEs and 1028 ± 45°C for amphiboles in the granite, respectively. However, the estimates are higher than the "amphibole saturation temperature" and the temperature of the amphibole from the host granite deviates from the amphibole stability field under most conditions (e.g., Xiong et al., 2005). On the other hand, the amphibole from the host granite crystallized earlier than that from the MMEs is unreasonable. This may be ascribed to that the Mg or Na exchange between the amphiboles and melts do not reach equilibrium, especially the Na in sodic amphiboles is under control of crystal chemistry. Thus, the temperature is more likely the closure temperature for element exchange to reach equilibrium other than the crystallization temperatures.

In summary, amphibole-only thermometers yield good results because the estimates are under "saturation temperature" but the thermometers also prove that the amphiboles crystallized as a late phase consistent with petrographic evidence. However, thermometers based on partition coefficients produce erroneous estimates.

The basis of amphiboles barometer is that Al-Tschermak exchange, which mainly involves in Al incorporation, is pressure-sensitive, so it seems to be proper to use Al to estimate pressure of crystallization (e.g., Hammarstrom and Zen, 1986; Shane and Smith, 2013; Mutch et al., 2016). However, most researchers have questioned the reliability of Al-in-amphiboles barometer, because the exchange of Al is also influenced by temperature and melt compositions, which means that variation of Al content of amphiboles is too complex to use for estimating pressure directly (e.g., Kiss et al., 2014). In order to acquire accurate pressure estimates, Anderson and Smith (1995) recommend two filters: $T < 800$°C and $Fe^{Amp}/(Fe^{Amp} + Mg^{Amp}) < 0.65$. If amphiboles fit these filters, they are suitable for Al-in-amphiboles barometer. Unfortunately, in our case, amphiboles in both the granite and MMEs are Fe-rich, far beyond the values required by the filters. On the other hand, Al content of amphiboles in our case are too low, which results in an unreasonably low pressure. In addition to Al-in-amphiboles barometer, Putirka (2016) recommended D_{Al} barometer to lower the uncertainty of pressure estimates, but no reasonable estimates can be acquired (10.5 kbar for amphiboles of MMEs; 3.5 kbar for amphiboles of granites). The outstanding pressure difference between the amphiboles from the MMEs and granites may also indicate that the estimates do not reflect depths but more related to temperature variations, which is consistent with the conclusion of Erdmann et al. (2014). Therefore, sodic amphiboles cannot be used to reflect the pressure change during magma mixing.

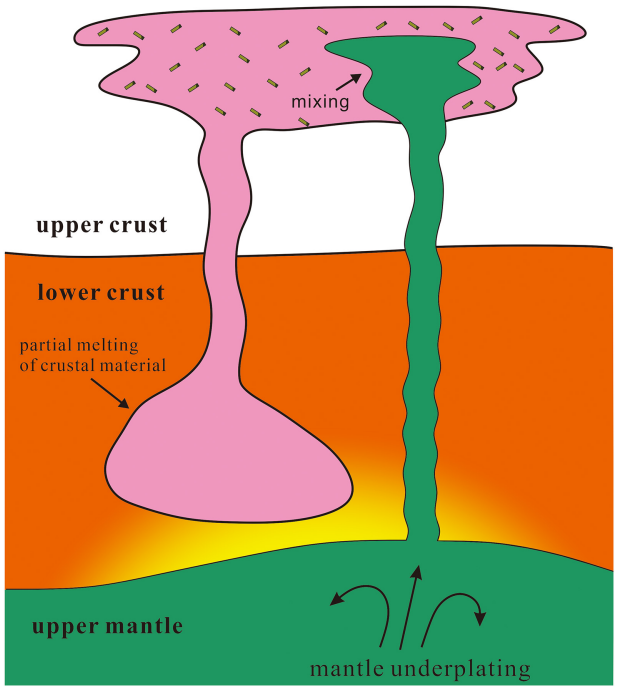

FIGURE 9 | Illustration of magma mixing during the formation of the Huangyangshan A-type granite and its MMEs (after Kemp et al., 2007).

CONCLUSION

We have shown major and trace elements variation of amphiboles of granites and MMEs during magma mixing and tentatively estimate the crystallization temperature and pressure of these amphiboles. In sodic amphiboles from both the MMEs and host granite, halogens in W-site and Mg, Fe, and Ti in C-site are only controlled by chemical compositions of magma and can potentially reflect the evolution of magma. By contrast, A-, B- and T-site cations are influenced by crystal chemistry and magma composition limiting their ability as tracers. Although F can depolymerize the melts, resulting in lower partition coefficients of trace elements, HFSE and REE behave more compatibly in sodic amphiboles than in calcic amphiboles. Also, taking "saturation temperature" as reference, amphiboles-only thermometers yield reasonable results and further prove amphiboles are later phase during magma mixing, but partition coefficient-based

thermometers show considerable deviation. All of the barometers now available rely on Al content or D_{Al} of amphiboles cannot be applied to Fe-rich and Al-poor amphiboles.

DATA AVAILABILITY STATEMENT

The original contributions presented in the study are included in the article/**Supplementary Material**, further inquiries can be directed to the corresponding author/s.

AUTHOR CONTRIBUTIONS

YF and CY together conceived the idea for this study. CY conducted petrographic observation, EPMA and LA-ICP-MS analyses on amphiboles, and wrote the manuscript. YF revised and finalized the manuscript. YF and RL conducted the fieldwork and collected the samples. GY provided assistance with the fieldwork. All authors contributed to the article and approved the submitted version.

FUNDING

This study is funded by the National Natural Science Foundation of China (grant numbers: 91962214 and 41902073) and Department of Science and Technology of Shaanxi Province (grant number: 2020JM-215).

ACKNOWLEDGMENTS

We are very grateful for the insightful suggestions from HL, FY, and ES that helped improve this manuscript. We would also like to thank XD for handling this manuscript.

SUPPLEMENTARY MATERIAL

The Supplementary Material for this article can be found online at: https://www.frontiersin.org/articles/10.3389/feart.2021.650014/full#supplementary-material

REFERENCES

Adam, J., Green, T. H., and Sie, S. H. (1993). Proton microprobe determined partitioning Of Rb, Sr, Ba, Y, Zr, Nb and Ta between experimentally produced amphiboles and silicate melts with variable F content. *Chem. Geol.* 109, 29–49. doi: 10.1016/0009-2541(93)90060-v

Anderson, J. L., and Smith, D. R. (1995). The effects of temperature and F(O2) on the al-in-hornblende barometer. *Am. Mineral.* 80, 549–559. doi: 10.2138/am-1995-5-614

Barbarin, B., and Didier, J. (1992). Genesis and evolution of mafic microgranular enclaves through various types of interaction between coexisting felsic and mafic magmas. *Trans. R. Soc. Edinburgh Earth Sci.* 83, 145–153. doi: 10.1017/s0263593300007835

Baxter, S., and Feely, M. (2002). Magma mixing and mingling textures in granitoids: examples from the Galway Granite, Connemara, Ireland. *Mineral. Petrol.* 76, 63–74.

Blundy, J., and Wood, B. (1994). Prediction of crystal-melt partition-coefficients from elastic-moduli. *Nature* 372, 452–454. doi: 10.1038/372452a0

Bonin, B. (2007). A-type granites and related rocks: evolution of a concept, problems and prospects. *Lithos* 97, 1–29. doi: 10.1016/j.lithos.2006.12.007

Bottazzi, P., Tiepolo, M., Vannucci, R., Zanetti, A., Brumm, R., Foley, S. F., et al. (1999). Distinct site preferences for heavy and light REE in amphibole and the prediction of D-Amph/L(REE). *Contrib. Mineral. Petrol.* 137, 36–45. doi: 10.1007/s004100050580

Brenan, J. M., Shaw, H. F., Ryerson, F. J., and Phinney, D. L. (1995). Experimental-determination of trace-element partitioning between pargasite and a synthetic hydrous andesitic melt. *Earth Planet. Sci. Lett.* 135, 1–11. doi: 10.1016/0012-821x(95)00139-4

Chappell, B. W., White, A. J. R., Williams, I. S., Wyborn, D., and Wyborn, L. A. I. (2000). Lachlan Fold Belt granites revisited: high- and low-temperature granites and their implications. *Aust. J. Earth Sci.* 47, 123–138. doi: 10.1046/j.1440-0952.2000.00766.x

Chen, B., Chen, Z. C., and Jahn, B. M. (2009). Origin of mafic enclaves from the Taihang Mesozoic orogen, north China craton. *Lithos* 110, 343–358. doi: 10.1016/j.lithos.2009.01.015

Dodge, F. C. W., and Kistler, R. W. (1990). Some additional observations on inclusions in the granitic-rocks of the sierra-nevada. *J. Geophys. Res. Solid Earth Planets* 95, 17841–17848. doi: 10.1029/jb095ib11p17841

Domanska-Siuda, J., Slaby, E., and Szuszkiewicz, A. (2019). Ambiguous isotopic and geochemical signatures resulting from limited melt interactions in a seemingly composite pluton: a case study from the Strzegom-Sobotka Massif (Sudetes, Poland). *Int. J. Earth Sci.* 108, 931–962. doi: 10.1007/s00531-019-01687-w

Erdmann, S., Martel, C., Pichavant, M., and Kushnir, A. (2014). Amphibole as an archivist of magmatic crystallization conditions: problems, potential, and implications for inferring magma storage prior to the paroxysmal 2010 eruption of Mount Merapi, Indonesia. *Contrib. Mineral. Petrol.* 167:1016.

Guo, F., Jiang, C., Lu, R., Xia, Z., Ling, J., and Guo, N. (2010). Petrogenesis of the Huangyangshan alkali granites in Kalamaili area, northern Xinjiang. *Acta Petrologica Sinica* 26, 2357–2373.

Hammarstrom, J. M., and Zen, E. A. (1986). Aluminum in hornblende - an empirical igneous geobarometer. *Am. Mineral.* 71, 1297–1313.

Hawthorne, F. C., Della Ventura, G., Oberti, R., Robert, J. L., and Iezzi, G. (2005). Short-range order in minerals: amphiboles. *Can. Mineral.* 43, 1895–1920. doi: 10.2113/gscanmin.43.6.1895

Hawthorne, F. C., Oberti, R., and Sardone, N. (1996). Sodium at the a site in clinoamphiboles: the effects of composition on patterns of order. *Can. Mineral.* 34, 577–593.

Hawthorne, F. C., Oberti, R., Harlow, G. E., Maresch, W. V., Martin, R. F., Schumacher, J. C., et al. (2012). Nomenclature of the amphibole supergroup. *Am. Mineral.* 97, 2031–2048. doi: 10.2138/am.2012.4276

Hawthorne, F. C., Ungaretti, L., Oberti, R., Bottazzi, P., and Czamanske, G. K. (1993). LI - AN important component in igneous alkali amphiboles. *Am. Mineral.* 78, 733–745.

Hawthorne, F. C., Ungaretti, L., Oberti, R., Cannillo, E., and Smelik, E. A. (1994). The mechanism Of 6 Li incorporation in amphiboles. *Am. Mineral.* 79, 443–451.

Huang, H., Niu, Y. L., Nowell, G., Zhao, Z. D., Yu, X. H., Zhu, D. C., et al. (2014). Geochemical constraints on the petrogenesis of granitoids in the East Kunlun Orogenic belt, northern Tibetan Plateau: implications for continental crust growth through syn-collisional felsic magmatism. *Chem. Geol.* 370, 1–18. doi: 10.1016/j.chemgeo.2014.01.010

Iveson, A. A., Rowe, M. C., Webster, J. D., and Neill, O. K. (2018). Amphibole-, Clinopyroxene- and Plagioclase-melt partitioning of trace and economic metals in halogen-bearing rhyodacitic melts. *J. Petrol.* 59, 1579–1604. doi: 10.1093/petrology/egy072

Iveson, A. A., Webster, J. D., Rowe, M. C., and Neill, O. K. (2017). Major Element and Halogen (F, Cl) mineral-melt-fluid partitioning in hydrous rhyodacitic melts at shallow crustal conditions. *J. Petrol.* 58, 2465–2492. doi: 10.1093/petrology/egy011

Kazemi, K., Kananian, A., Xiao, Y., and Sarjoughian, F. (2019). Petrogenesis of Middle-Eocene granitoids and their Mafic microgranular enclaves in central

Urmia-Dokhtar Magmatic Arc (Iran): evidence for interaction between felsic and mafic magmas. *Geosci. Front.* 10, 705–723. doi: 10.1016/j.gsf.2018.04.006

Kemp, A. I. S., Hawkesworth, C. J., Foster, G. L., Paterson, B. A., Woodhead, J. D., Hergt, J. M., et al. (2007). Magmatic and crustal differentiation history of granitic rocks from Hf-O isotopes in zircon. *Science* 315, 980–983. doi: 10.1126/science.1136154

Kiss, B., Harangi, S., Ntaflos, T., Mason, P. R. D., and Pal-Molnar, E. (2014). Amphibole perspective to unravel pre-eruptive processes and conditions in volcanic plumbing systems beneath intermediate arc volcanoes: a case study from Ciomadul volcano (SE Carpathians). *Contrib. Mineral. Petrol.* 167:986.

Kumar, S., and Rino, V. (2006). Mineralogy and geochemistry of microgranular enclaves in Palaeoproterozoic Malanjkhand granitoids, central India: evidence of magma mixing, mingling, and chemical equilibration. *Contrib. Mineral. Petrol.* 152, 591–609. doi: 10.1007/s00410-006-0122-3

Kumar, S., Rino, V., and Pal, A. B. (2004). Typology and geochemistry of microgranular enclaves hosted in Malanjkhand Granitolds, central India. *J. Geol. Soc. India* 64, 277–292.

Leake, B. E., Woolley, A. R., Arps, C. E. S., Birch, W. D., Gilbert, M. C., and Grice, J. D. (1997). Nomenclature of amphiboles: report of the subcommittee on amphiboles of the international mineralogical association, commission on new minerals and mineral names. *Am. Mineral.* 82, 1019–1037.

Liu, L., Qiu, J.-S., and Li, Z. (2013). Origin of mafic microgranular enclaves (MMEs) and their host quartz monzonites from the Muchen pluton in Zhejiang province, Southeast China: implications for magma mixing and crust-mantle interaction. *Lithos* 160, 145–163. doi: 10.1016/j.lithos.2012.12.005

Locock, A. J. (2014). An excel spreadsheet to classify chemical analyses of amphiboles following the IMA 2012 recommendations. *Comput. Geosci.* 62, 1–11. doi: 10.1016/j.cageo.2013.09.011

Ma, X., Chen, B., and Yang, M. (2013). Magma mixing origin for the Aolunhua porphyry related to Mo-Cu mineralization, eastern central Asian Orogenic Belt. *Gondwana Res.* 24, 1152–1171. doi: 10.1016/j.gr.2013.02.010

Marks, M., Halama, R., Wenzel, T., and Markl, G. (2004). Trace element variations in clinopyroxene and amphibole from alkaline to peralkaline syenites and granites: implications for mineral-melt trace-element partitioning. *Chem. Geol.* 211, 185–215. doi: 10.1016/j.chemgeo.2004.06.032

Molina, J. F., Moreno, J. A., Castro, A., Rodriguez, C., and Fershtater, G. B. (2015). Calcic amphibole thermobarometry in metamorphic and igneous rocks: new calibrations based on plagioclase/amphibole Al-Si partitioning and amphibole/liquid Mg partitioning. *Lithos* 232, 286–305. doi: 10.1016/j.lithos.2015.06.027

Morrison, J. (1991). Compositional constraints on the incorporation of Cl into Amphiboles. *Am. Mineral.* 76, 1920–1930.

Mutch, E. J. F., Blundy, J. D., Tattitch, B. C., Cooper, F. J., and Brooker, R. A. (2016). An experimental study of amphibole stability in low-pressure granitic magmas and a revised Al-in-hornblende geobarometer. *Contrib. Mineral. Petrol.* 171:85.

Oberti, R., Camara, F., Ottolini, L., and Caballero, J. M. (2003). Lithium in amphiboles: detection, quantification, and incorporation mechanisms in the compositional space bridging sodic and Li-B-amphiboles. *Eur. J. Mineral.* 15, 309–319. doi: 10.1127/0935-1221/2003/0015-0309

Oberti, R., Ungaretti, L., Cannillo, E., and Hawthorne, F. C. (1992). the behavior of ti in amphiboles .1. 4-coordinate and 6-coordinate ti in richterite. *Eur. J. Mineral.* 4, 425–439. doi: 10.1127/ejm/4/3/0425

Paton, C., Hellstrom, J., Paul, B., Woodhead, J., and Hergt, J. (2011). Iolite: freeware for the visualisation and processing of mass spectrometric data. *J. Anal. At. Spectrom.* 26, 2508–2518. doi: 10.1039/c1ja10172b

Price, J. D., Hogan, J. P., Gilbert, M. C., London, D., and Morgan, G. B. (1999). Experimental study of titanite-fluorite equilibria in the A-type mount scott granite: implications for assessing F contents of felsic magma. *Geology* 27, 951–954. doi: 10.1130/0091-7613(1999)027<0951:esotfe>2.3.co;2

Putirka, K. (2016). Amphibole thermometers and barometers for igneous systems and implications for eruption mechanisms of felsic magmas at arc volcanoes. *Am. Mineral.* 101, 841–858. doi: 10.2138/am-2016-5506

Renna, M. R., Tribuzio, R., and Tiepolo, M. (2006). Interaction between basic and acid magmas during the latest stages of the post-collisional variscan evolution: clues from the gabbro-granite association of Ota (Corsica-Sardinia batholith). *Lithos* 90, 92–110. doi: 10.1016/j.lithos.2006.02.003

Ridolfi, F., and Renzulli, A. (2012). Calcic amphiboles in calc-alkaline and alkaline magmas: thermobarometric and chemometric empirical equations valid up to 1,130A degrees C and 2.2 GPa. *Contrib. Mineral. Petrol.* 163, 877–895. doi: 10.1007/s00410-011-0704-6

Ridolfi, F., Renzulli, A., and Puerini, M. (2010). Stability and chemical equilibrium of amphibole in calc-alkaline magmas: an overview, new thermobarometric formulations and application to subduction-related volcanoes. *Contrib. Mineral. Petrol.* 160, 45–66. doi: 10.1007/s00410-009-0465-7

Roberts, M. P., and Clemens, J. D. (1993). origin of high-potassium, calc-alkaline, i-type granitoids. *Geology* 21, 825–828. doi: 10.1130/0091-7613(1993)021<0825:oohpta>2.3.co;2

Scaillet, B., and MacDonald, R. (2001). Phase relations of peralkaline silicic magmas and petrogenetic implications. *J. Petrol.* 42, 825–845. doi: 10.1093/petrology/42.4.825

Schiano, P., Monzier, M., Eissen, J. P., Martin, H., and Koga, K. T. (2010). Simple mixing as the major control of the evolution of volcanic suites in the Ecuadorian Andes. *Contrib. Mineral. Petrol.* 160, 297–312. doi: 10.1007/s00410-009-0478-2

Sengor, A. M. C., Natalin, B. A., and Burtman, V. S. (1993). evolution of the altaid tectonic collage and paleozoic crustal growth in eurasia. *Nature* 364, 299–307. doi: 10.1038/364299a0

Shane, P., and Smith, V. C. (2013). Using amphibole crystals to reconstruct magma storage temperatures and pressures for the post-caldera collapse volcanism at Okataina volcano. *Lithos* 156, 159–170. doi: 10.1016/j.lithos.2012.11.008

Shannon, R. D. (1976). revised effective ionic-radii and systematic studies of interatomic distances in halides and chalcogenides. *Acta Crystallogr. Sec. A* 32, 751–767. doi: 10.1107/s0567739476001551

Shellnutt, J. G., Jahn, B. M., and Dostal, J. (2010). Elemental and Sr-Nd isotope geochemistry of microgranular enclaves from peralkaline A-type granitic plutons of the Emeishan large igneous province, SW China. *Lithos* 119, 34–46. doi: 10.1016/j.lithos.2010.07.011

Shimizu, K., Liang, Y., Sun, C., Jackson, C. R. M., and Saal, A. E. (2017). Parameterized lattice strain models for REE partitioning between amphibole and silicate melt. *Am. Mineral.* 102, 2254–2267. doi: 10.2138/am-2017-6110

Siegel, K., Williams-Jones, A. E., and van Hinsberg, V. J. (2017). The amphiboles of the REE-rich A-type peralkaline strange lake pluton fingerprints of magma evolution. *Lithos* 288, 156–174. doi: 10.1016/j.lithos.2017.07.012

Su, Y., Tang, H., and Cong, F. (2008). zircon u-pb age and petrogenesis of the huangyangshan alkalinegranite body in east junggar, xinjiang. *Acta Mineral. Sinica* 28, 117–126.

Sun, S. S., and McDonough, W. F. (1989). "Chemical and isotopic systematics of oceanic basalts: implications for mantle composition and processes," in *Magmatism in the Oceanic Basalts, Special Publication*, eds A. D. Saunders, and M. J. Norry (London: Geological Society), 313–345.

Tang, H., Qu, W., Su, Y., Hou, G., Du, A., and Cong, F. (2007). Genetic connection of Sareshike tin deposit with the alkaline A-type granites of sabei body in Xinjiang: constraint from isotopic ages. *Acta Petrologica Sinica* 23, 1989–1997.

Tiepolo, M., Bottazzi, P., Foley, S. F., Oberti, R., Vannucci, R., and Zanetti, A. (2001). Fractionation of Nb and Ta from Zr and Hf at mantle depths: the role of titanian pargasite and kaersutite. *J. Petrol.* 42, 221–232. doi: 10.1093/petrology/42.1.221

Tiepolo, M., Oberti, R., Zanetti, A., Vannucci, R., and Foley, S. F. (2007). "Trace-element partitioning between amphibole and silicate melt," in *Amphiboles: Crystal Chemistry, Occurrence, and Health Issue*, eds F. C. Hawthorne, R. Oberti, G. DellaVentura, and A. Mottana (Berlin: De Gruyter), 417–451. doi: 10.2138/rmg.2007.67.11

Van den Bleeken, G., and Koga, K. T. (2015). Experimentally determined distribution of fluorine and chlorine upon hydrous slab melting, and implications for F-Cl cycling through subduction zones. *Geochimica Et Cosmochimica Acta* 171, 353–373. doi: 10.1016/j.gca.2015.09.030

White, A. J. R., and Chappell, B. W. (1977). ultrametamorphism and granitoid genesis. *Tectonophysics* 43, 7–22. doi: 10.1016/0040-1951(77)90003-8

White, A. J. R., Chappell, B. W., and Wyborn, D. (1999). Application of the restite model to the Deddick Granodiorite and its enclaves - a reinterpretation of the observations and data of Maas et al. (1997). *J. Petrol.* 40, 413–421. doi: 10.1093/petroj/40.3.413

Wiebe, R. A., Smith, D., Sturm, M., King, E. M., and Seckler, M. S. (1997). Enclaves in the cadillac mountain granite (coastal Maine): samples of hybrid magma from the base of the chamber. *J. Petrol.* 38, 393–423. doi: 10.1093/petroj/38.3.393

Xiao, W. J., Windley, B. F., Hao, J., and Zhai, M. G. (2003). Accretion leading to collision and the permian solonker suture, inner mongolia, China: termination of the central Asian orogenic belt. *Tectonics* 22. doi: 10.1029/2002tc001484

Xiong, X. L., Adam, J., and Green, T. H. (2005). Rutile stability and rutile/melt HFSE partitioning during partial melting of hydrous basalt: implications for TTG genesis. *Chem. Geol.* 218, 339–359. doi: 10.1016/j.chemgeo.2005.01.014

Xiong, X., Zhu, L., Zhang, G., Santosh, M., Jiang, H., Zheng, J., et al. (2020). Petrogenesis and tectonic implications of Indosinian granitoids from Western Qinling Orogen, China: Products of magma-mixing and fractionation. *Geosci. Front.* 11, 1305–1321. doi: 10.1016/j.gsf.2019.12.011

Yang, G., Li, Y., Wu, H., Si, G., Jin, Z., and Zhang, Y. (2009). LA-ICP-MS zircon U-Pb dating of the huangyangshan pluton and its enclaves from kalamaili area eastern Junggar, Xinjiang, and geological implications. *Acta Petrologica Sinica* 25, 3197–3207.

Yang, G., Li, Y., Wu, H., Si, G., Zhang, Y., and Jin, Z. (2010). A tentative discussion on the genesis of huangyangshan granite body in kalamaili orogen,east junggar. *Acta Geoscientia Sinica* 31, 170–182.

Yang, G., Li, Y., Wu, H., Zhong, X., Yang, B., Yan, C., et al. (2011). Geochronological and geochemical constrains on petrogenesis of the Huangyangshan A-type granite from the East Junggar, Xinjiang, NW China. *J. Asian Earth Sci.* 40, 722–736. doi: 10.1016/j.jseaes.2010.11.008

Yang, J.-H., Wu, F.-Y., Chung, S.-L., Wilde, S. A., and Chu, M.-F. (2004). Multiple sources for the origin of granites: geochemical and Nd/Sr isotopic evidence from the gudaoling granite and its mafic enclaves, northeast China. *Geochimica Et Cosmochimica Acta* 68, 4469–4483. doi: 10.1016/j.gca.2004.04.015

Yang, J.-H., Wu, F.-Y., Chung, S.-L., Wilde, S. A., and Chu, M.-F. (2006). A hybrid origin for the Qianshan A-type granite, northeast China: geochemical and Sr-Nd-Hf isotopic evidence. *Lithos* 89, 89–106. doi: 10.1016/j.lithos.2005.10.002

Zorpi, M. J., Coulon, C., Orsini, J. B., and Cocirta, C. (1989). magma mingling, zoning and emplacement in calc-alkaline granitoid plutons. *Tectonophysics* 157, 315–329. doi: 10.1016/0040-1951(89)90147-9

Conflict of Interest: The authors declare that the research was conducted in the absence of any commercial or financial relationships that could be construed as a potential conflict of interest.

Copyright © 2021 Ye, Feng, Lei and Yang. This is an open-access article distributed under the terms of the Creative Commons Attribution License (CC BY). The use, distribution or reproduction in other forums is permitted, provided the original author(s) and the copyright owner(s) are credited and that the original publication in this journal is cited, in accordance with accepted academic practice. No use, distribution or reproduction is permitted which does not comply with these terms.